

THERMAL-ECONOMIC MULTI-OBJECTIVE OPTIMIZATION OF HEAT PIPE HEAT EXCHANGER FOR ENERGY RECOVERY IN HVAC APPLICATION USING GENETIC ALGORITHM

by

Sepehr SANAYE* and Davood MODARRESPOOR

Energy Systems Improvement Laboratory, Mechanical Engineering Department,
Iran University of Science and Technology, Narmak, Tehran, Iran

Original scientific paper
DOI: 10.2298/TSCI111024203S

Cost and effectiveness are two important factors of heat pipe heat exchanger design. The total cost includes the investment cost for buying equipment (heat exchanger surface area) and operating cost for energy expenditures (related to fan power). The heat pipe heat exchanger was thermally modeled using ε -NTU method to estimate the overall heat transfer coefficient for the bank of finned tubes as well as estimating pressure drop. Fast and elitist non-dominated sorting genetic algorithm II with continuous and discrete variables was applied to obtain the maximum effectiveness and the minimum total cost as two objective functions. Pipe diameter, pipe length, numbers of pipes per row, number of rows, fin pitch and fin length ratio were considered as six design parameters. The results of optimal designs were a set of multiple optimum solutions, called "Pareto optimal solutions". The comparison of the optimum values of total cost and effectiveness, variation of optimum values of design parameters as well as estimating the pay-back period were also reported for various inlet fresh air volume flow rates.

Keywords: heat pipe heat exchanger, heat recovery, effectiveness, total cost, multi-objective optimization, non-dominated sorting genetic algorithm

Introduction

Due to continuous increase of fuel cost, heat recovery in HVAC systems has been focused by many researchers. The waste energy of exhaust air can be recovered by using a heat exchanger. Heat pipe heat exchangers have many advantages over other conventional ones; large quantities of heat transported through a small cross-sectional area, no required additional power input (except for the fans to drive the airstreams), low pressure drop, high reliability and simple structure are some examples [1, 2]. Yau [3] experimentally studied 8-row thermo syphon-based heat pipe heat exchanger for building HVAC systems in tropical regions and investigated the influence of the inlet air dry-bulb temperature, relative humidity and air velocity on the sensible heat. Noie-Baghban and Majideian [4] designed, manufactured and tested a heat pipe heat exchanger (HPHE) for heat recovery of surgery rooms with three types of wick and three working fluids. Abd El-Baky and Mohamed [5] also used HPHE for heat recovery of exhaust air. Different ratios of mass flow rate and different inlet air temperatures were tested to investigate the effectiveness and heat recovery of HPHE. Peretz and Benoescu [6] analyzed the effectiveness of a series of HPHE, with different number of rows in depth,

*Corresponding author; e-mail: sepehr@iust.ac.ir

various frontal surface areas as well as the fin density. Tan *et al.* [7] proposed the optimum position of the partition separating a heat pipe into evaporator and condenser regions in a heat pipe heat exchanger by minimizing the total thermal resistance. In a thermal-economical optimization of HPHE Soylemez [8] estimated the optimum HPHE effectiveness for energy recovery applications. Peretz and Horbaniuc [9] optimized a HPHE with continuous planar fins and a staggered equilateral triangular tube pitch to maximize heat transfer rate. Sanaye and Hajabdollahi [10] used NSGA-II to optimize a shell and tube heat exchanger.

In this paper after thermal modeling of a HPHE using ε -NTU method, it was optimized by maximizing the effectiveness as well as minimizing the total cost. Genetic algorithm optimization technique was applied to provide a set of Pareto multiple optimum solutions. The payback period and annular heat recovery were calculated for five different inlet fresh air volume flow rates. Finally to insure the heat pipe performance the heat pipe heat transfer limitations were investigated.

The followings are the contribution of this paper into the subject.

- Applying multi-objective optimization of HPHE with effectiveness and total cost as two objectives (not considered previously in open literature) using genetic algorithm. The imposed constraints included both pressure drop and heat transfer limitations were imposed in the optimization procedure in the evaporator and condenser.
- Selecting six design parameters (decision variables) including two fin characteristics, *i. e.* the fin pitch and fin height ratio as well as four parameters relevant to the heat exchanger geometry such as pipe diameter, number of pipes per row, number of rows and the pipe length.
- Proposing a closed form equation for the total cost in terms of effectiveness at the optimal design point.
- Comparison of the total cost, effectiveness and variation of optimum values of design parameters at the optimum design points for various inlet fresh air volume flow rates.

Performing the payback period analysis of equilibrium points for various inlet fresh air volume flow rates.

Thermal modeling

Air conditioning system

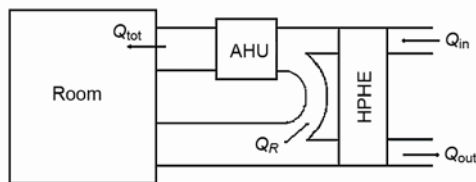


Figure1. The schematic of the studied air conditioning system with HPHE installed

Figure 1 shows the schematic of the studied system including the HPHE installed at the exhaust and inlet air path and return air flow duct. In order to have air with the desired quality, a fraction of return air is mixed with the inlet fresh air and enters the air handling unit (AHU). The HPHE recovers the exhaust air heat and transfers it to the cold inlet fresh air in the heating mode and preheats the inlet fresh air while it recovers the exhaust cold air energy and precools the warm inlet fresh air in the cooling mode. This reduces the heating and cooling load of the AHU compared with the system in which HPHE is not installed.

The required inlet fresh air volume flow rates to provide the condition of human comfort in summer and winter was considered equal to Q_s and Q_w in the cooling and heating mode, respectively. The inside room air temperature is T_R , inlet air temperature at the entrance

of the heat exchanger is the average of the temperature of the days with maximum temperature in the summer and temperature of the days with the lowest temperature in the winter for the desired place. Outlet air temperature entering the heat exchanger due to losses is less than T_R in the heating operation mode and more than T_R in the cooling operation mode.

The heat pipe performance

Generally there are some maximum heat transfer rate limitations in heat pipes that can be divided into two primary categories: limits that result in heat pipe failure and limits that do not. For the limitations resulting in heat pipe failure such as capillary, entrainment and boiling limitations, there exists insufficient liquid flow to the evaporator for a given heat input absorbed, thus resulting in dryout of the evaporator wick structure. However, limitations not resulting the heat pipe failure such as viscous and sonic limitations require that the heat pipe operate at an increased temperature when the absorbed heat increases [11].

For a heat pipe to work properly the net capillary pressure difference produced in the wick structure must be greater than the summation of all the losses occurring throughout the liquid and vapor flow paths. This relationship, referred to as the capillary limitation, can be expressed as [10]:

$$\Delta P_{\text{cap}} \geq \Delta P_l + \Delta P_v + \Delta P_g \quad (1)$$

where $\Delta P_{\text{cap}} = 2\sigma/r_{\text{cap}}$ is the maximum capillary pressure difference generated within the wick structure, estimated from [10], σ – the working fluid surface tension, and $r_{\text{cap}} = 1/(2N_{\text{mesh}})$ – the capillary radius for the wicking structure, and N_{mesh} – the screen mesh number.

ΔP_l is the total pressure drop in the liquid phase, in from of [12]:

$$\Delta P_l = \frac{\mu_l L_{\text{eff}} q_{\text{cap}}}{K_{\text{per}} \rho_l h_{\text{fg}} A_{\text{wi}}} \quad \text{and} \quad K_{\text{per}} = \frac{d_{\text{wi}}^2 \phi^3}{122(1-\phi)^2} \quad (2)$$

where ρ_l and μ_l are the density and viscosity of working fluid in liquid phase, A_{wi} is the wick cross-section area, q_{cap} – the maximum axial heat transport of heat pipe due to capillary limitation, and K_{per} – the wick permeability estimated for wrapped, d_{wi} – the wire diameter, and ϕ – the wick porosity determined for screened wicks [12].

ΔP_v is the total pressure drop in vapor phase, in from of [12]:

$$\Delta P_v = \left[\frac{C(f_v Re_v) \mu_v}{2r_v^2 A_v \rho_v h_{\text{fg}}} \right] L_{\text{eff}} q_{\text{cap}} \quad (3)$$

where h_{fg} is the working fluid latent heat of vaporization, A_v and r_v are vapor flow cross-section area and radius, respectively, ρ_v and μ_v are the density and viscosity of vapor flow, C and f_v are parameters determined using vapor flow Reynolds and Mach numbers, $L_{\text{eff}} = (L_e + L_c)/2 + L_{\text{ad}}$ is effective length of the heat pipe while L_e and L_c are evaporator and condenser lengths and L_{ad} is the adiabatic section length.

ΔP_g is the hydrostatic pressure drop due to gravity [12]:

$$\Delta P_g = \rho_l g L_1 \sin \psi + \rho_l g d_v \cos \psi \quad (4)$$

where L_1 is the heat pipe length and ψ – the slope angle of heat pipe makes with horizontal axis.

By computing each pressure drop term in eq. (1), the heat pipe heat transfer capacity rate could be estimated for various working fluids and wick structures.

At higher heat fluxes, nucleate boiling may occur in the wick structure, which may allow vapor to become trapped in the wick, thus blocking liquid return and resulting in evaporator dryout. This phenomenon, referred to as the boiling limit could be estimated from [11, 12]:

$$q_b = \left[\frac{2\pi L_e k_{\text{eff}} T_v}{h_{\text{fg}} \rho_v \ln(r_i/r_v)} \right] \left(\frac{2\sigma}{r_n} - \Delta P_{\text{cap}} \right) \quad (5)$$

where T_v is the vapor temperature, k_{eff} – the effective thermal conductivity of saturated wick, and r_n – the nucleation site radius which was assumed to be $2.54 \cdot 10^{-7}$ m in our case study [10].

Examination of the basic flow conditions in a heat pipe shows that the liquid and vapor flow in opposite directions. The interaction between the countercurrent liquid and vapor flow results in viscous shear forces occurring at the liquid-vapor interface, which may inhibit liquid return to the evaporator and is referred to as entrainment limit expressed as [12]:

$$q_{\text{ent}} = h_{\text{fg}} A_v \left(\frac{\rho_v \sigma}{2r_{h,w}} \right)^{0.5} \quad (6)$$

where $r_{h,w}$ is the hydraulic radius of the wick structure.

The sonic limit is typically experienced in liquid metal heat pipes during startup or low-temperature operation due to the associated very low vapor densities in this condition. This may result in choked, or sonic, vapor flow. For most heat pipes operating at room temperature or cryogenic temperatures, the sonic limit will not typically occur, except in the case of very small vapor channel diameters [11]. The maximum heat transfer rate was computed in this case from [10]:

$$q_S = \rho_v h_{\text{fg}} A_v \left[\frac{\gamma_v R_v T_v}{2(\gamma_v + 1)} \right]^{0.5} \quad (7)$$

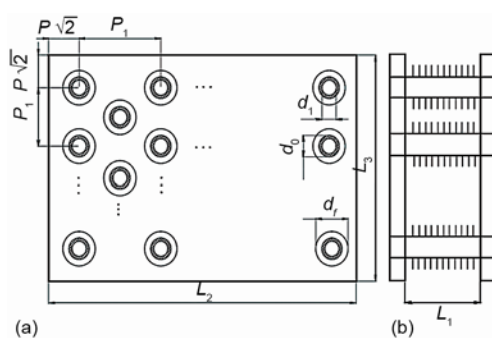


Figure 2. The schematic of the HPHE staggered finned tube arrangement (a) top view (b) side view

Heat transfer surface area of a single pipe A_{tot} , is the sum of finned (A_f) and unfinned (A_p) surface areas:

where γ_v is the vapor specific heat which for tri-atomic fluids was considered to be 1.33 [10].

HPHE system

As illustrated in fig. 2, for the staggered pipe arrangement with circular fins and the shown geometrical specifications the total number of pipes in the HPHE is:

$$N_{\text{tot}} = \frac{L_2 L_3}{P_1 P_1} = N_T N_L \quad (8a)$$

where N_T and N_L are number of pipes per row and number of rows, respectively.

$$A_{\text{tot}} = A_p + A_f, \quad A_p = \pi d_o (L_1 - t_f N_f L_1), \quad A_f = \left[2\pi \frac{(d_f^2 - d_o^2)}{4} + \pi d_f t_f \right] L_1 N_f \quad (8b)$$

The minimum free flow area is [13]:

$$A_{\text{fr}} = \left[\left(\frac{L_3}{P_T} - 1 \right) z + (P_T - d_o) - (d_f - d_o) t_f N_f \right] L_1 \quad (8c)$$

where

$$z = \begin{cases} 2x & \text{if } x < y \\ 2y & \text{if } x > y \end{cases}, \quad x = \frac{1}{2} [(P_T - d_o) - (d_f - d_o) t_f N_f],$$

$$y = \sqrt{\left(\frac{P_T}{2} \right)^2 + P_L^2 - d_o - (d_f - d_o) t_f N_f}$$

Other heat exchanger dimensions as shown in fig. 2 are $L_2 = N_L P_L$ and $L_3 = N_T P_T$, where N_T and N_L are number of pipes per row and number of rows, respectively. P_T and P_L are transverse and longitudinal pipe pitch.

ε -NTU method is used to predict the effectiveness of the HPHE. Heat exchanger effectiveness ε is defined as the ratio of the actual to the maximum heat transfer rate in a heat exchanger [14]:

$$\varepsilon = \frac{q}{q_{\text{max}}} = \frac{C_e (T_{e,\text{in}} - T_{e,\text{out}})}{C_{\text{min}} (T_{e,\text{in}} - T_{c,\text{in}})} = \frac{C_c (T_{c,\text{out}} - T_{c,\text{in}})}{C_{\text{min}} (T_{h,\text{in}} - T_{c,\text{in}})} \quad (9)$$

where q is the actual heat transfer, $C_e = (\dot{m} C_p)_e$ and $C_c = (\dot{m} C_p)_c$ are the heat capacity of the hot and cold flows, respectively. C_{min} is the minimum of C_e and C_c . The subscripts h and c refer to evaporator and condenser section of the heat pipe.

The effectiveness of the evaporator and condenser section of the heat pipe can be estimated from [15]:

$$\varepsilon_e = 1 - e^{-NTU_e}, \quad \varepsilon_c = 1 - e^{-NTU_c} \quad (10)$$

where

$$NTU_e = \frac{U_e A_e}{C_e}, \quad NTU_c = \frac{U_c A_c}{C_c} \quad (11)$$

U_e and U_c are the overall heat transfer coefficients in the high and low temperature side, A_e and A_c are the heat transfer surface areas of the evaporator and condenser sections including finned surfaces.

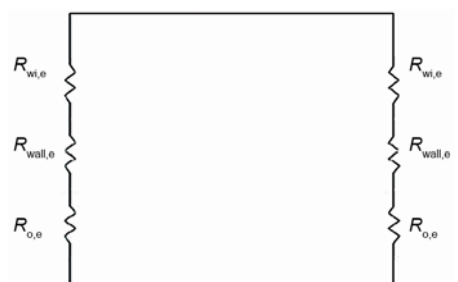
For an individual heat pipe the effectiveness is estimated as [16]:

$$\varepsilon_p = \left(\frac{1}{\varepsilon_{\text{min}}} + \frac{C^*}{\varepsilon_{\text{max}}} \right)^{-1} \quad (12)$$

where ε_{min} and ε_{max} are the minimum and maximum values of ε_e and ε_c , respectively. The heat capacity ratio C^* is:

$$C^* = \frac{C_{\min}}{C_{\max}} \quad (13)$$

For a multistage heat pipe heat exchanger in which there are a number of columns each containing a row of heat pipes (normal to the flow), the effectiveness is determined by [16]:



$$\varepsilon = \frac{\left(\frac{1 - C^* \varepsilon_p}{1 - \varepsilon_p} \right) - 1}{\left(\frac{1 - C^* \varepsilon_p}{1 - \varepsilon_p} \right) - C^*} \quad (14)$$

Figure 3. Equivalent thermal resistance of a heat pipe

By definition of the overall heat transfer coefficients in terms of thermal resistances for the evaporator and condenser section and by assuming negligible axial heat conduction through the heat pipes wall (fig. 3) [15]:

$$\frac{1}{(UA)_e} = R_{o,e} + R_{wall,e} + R_{wi,e}, \quad \frac{1}{(UA)_c} = R_{o,c} + R_{wall,c} + R_{wi,c} \quad (15)$$

where $R_{o,e}$ and $R_{o,c}$ are the thermal resistances due to convective heat transfer at the outer surface of the evaporator and condenser sections [14]:

$$R_{o,e} = \frac{1}{(\eta_o hA)_e}, \quad R_{o,c} = \frac{1}{(\eta_o hA)_c} \quad (16)$$

for extended surfaces η_o is the overall fin efficiency and h is the convective heat transfer coefficient. Furthermore $R_{wall,e}$ and $R_{wall,c}$ are the thermal resistances of circular pipe wall which are estimated from [14]:

$$R_{wall,e} = \frac{1}{2\pi k_{wall} L_e} \ln \left(\frac{d_o}{d_i} \right), \quad R_{wall,c} = \frac{1}{2\pi k_{wall} L_c} \ln \left(\frac{d_o}{d_i} \right) \quad (17)$$

$R_{wi,h}$ and $R_{wi,c}$ are thermal resistances of liquid saturated wick [12,17]:

$$R_{wi,e} = \frac{t_{wi}}{k_{eff} A_{i,e}}, \quad R_{wi,c} = \frac{t_{wi}}{k_{eff} A_{i,c}} \quad (18)$$

where t_{wi} is the wick thickness and k_{eff} — the effective thermal conductivity of the liquid saturated wick.

Convective heat transfer coefficient for the tube bank with individually circular finned tubes was estimated from [13]:

$$Nu = \frac{hd_o}{k_{air}} = 0.134 Re_d^{0.681} \left(\frac{s}{L_f} \right)^{0.2} \left(\frac{s}{t_f} \right)^{0.1134} \quad (19)$$

where $s = 1/N_f - t_f$.

Reynolds number Re_d is based on the outside tube diameter, L_f is the fin height, t_f – the fin thickness, and N_f – the number of fins per unit length. This is applicable for the following parameter definitions:

$$0.09 \leq \frac{L_f}{d_o} \leq 0.69, \quad 0.011 \leq \frac{t_f}{d_o} \leq 0.15, \quad 11.1 \leq d_o \leq 40.9 \text{ m}, \quad 246 \leq N_f \leq 768$$

The fin efficiency for circular fins was estimated from [13]:

$$\eta_f = \frac{\tanh\left(\sqrt{\frac{2h}{k_f t_f}} l^*\right)}{\sqrt{\frac{2h}{k_f t_f}} l^*}, \quad l^* = (r_f - r_o) \left[1 + \frac{t_f}{2(r_f - r_o)}\right] \left[1 + 0.3 \ln\left(\frac{r_f}{r_o}\right)\right] \quad (20)$$

where r_f is the fin outer diameter.

The overall fin efficiency is [15]:

$$\eta_o = 1 - \frac{A_f}{A_{tot}} (1 - \eta_f) \quad (21)$$

The amount of heat recovered in the HPHE:

$$q_{re} = \varepsilon C_{\min} (T_{e,in} - T_{c,in}) \quad (22)$$

The pressure drop for flow through a tube bank with individually finned tube [16]:

$$\Delta P = 2N_L f \frac{G^2}{\rho_{in}} + G^2 \left(\frac{1}{\rho_{out}} - \frac{1}{\rho_{in}} \right) \quad (23)$$

where the mass flow velocity G is based on the minimum free flow area, $G = \dot{m}/A_{ff}$.

The friction factor was also estimated from [13]:

$$f = 9.465 Re_d^{-0.316} \left(\frac{P_T}{d_o} \right)^{-0.937} \quad (24)$$

applicable for:

$$0.09 \leq \frac{L_f}{d_o} \leq 0.69, \quad 1.8 \leq \frac{P_T}{d_o}, \quad \frac{P_L}{d_o} \leq 4.6, \quad 18.6 \leq d_o \leq 40.9 \text{ mm}, \quad 311 \leq N_f \leq 431$$

Economic analysis

The total cost includes investment cost and operating cost of fan to flow the air over the finned tubes [8]:

$$C_{tot} = P_A C_A A_{HX} + PWFC_{op} \quad (25)$$

where C_A is the area dependent cost, A_{HX} – the heat transfer surface area, C_{op} – the total operation cost, and PWF – the present worth factor defined as [18]:

$$PWF(N_y, i, ds) = \begin{cases} \frac{1}{ds - i} \left[1 - \left(\frac{1+i}{1+ds} \right)^{N_y} \right] & \text{if } (i \neq ds) \\ \frac{N_y}{1+i} & \text{if } (i = ds) \end{cases} \quad (25a)$$

where N_y is the technical life of the HPHE and P_A – the ratio of the life cycle cost of the heat recovery system to its initial cost estimated as [18]:

$$P_A = 1 + PWF M_S - \frac{Rv}{(1+ds)^{N_y}} \quad (25b)$$

where M_S is the ratio of annual maintenance and miscellaneous expenditures to the original initial cost, Rv – the ratio of resale value to the initial cost, i – the inflation rate, and ds – the discount rate.

Total operation cost can be written as:

$$C_{op} = PWF C_{el} Q_{in} \frac{\Delta P_s H_s + \Delta P_w H_w}{\eta_{fan}} \quad (26)$$

where C_{el} is the electricity unit cost, \$/MWh, η_{fan} – the fan efficiency, H – the total working hours, and the subscripts s and w refer to summer and winter.

Energy recovered in cooling and heating modes could be converted to its monetary value and the net present worth (NPW) is defined as the difference between the total costs of a conventional fuel-only system and the recovered energy cost [18]:

$$NPW = PWF \left[C_{el} \frac{(q_{re}H)_s}{COP} + C_{eg} \frac{(q_{re}H)_w}{\rho_{fl} LHV \eta_b} \right] - C_{tot} \quad (27)$$

where ρ_{fl} is the methane density at the atmospheric temperature, LHV – the lower heating value of methane, and C_{eg} is the gas price, \$/m³, η_b – the boiler efficiency, and COP is the coefficient of performance of refrigeration cycle.

Payback period (N_p) is defined as the time needed for the cumulative fuel savings to equal the total initial investment, that is, how long it takes to get an investment back by saving in fuel [18] and can be obtained by equating net present worth (eq. 27) to zero and substituting N_p for PWF in eq. (25a):

$$N_p = \begin{cases} \frac{\ln \left[1 + (i - ds) \frac{C_{tot}}{C_{fl}} \right]}{\ln \left(\frac{1+i}{1+ds} \right)} & \text{if } (i \neq ds) \\ (1+i) \frac{C_{tot}}{C_{fl}} & \text{if } (i = ds) \end{cases}, \quad C_{fl} = C_{el} \frac{(q_{re}H)_s}{COP} + C_{eg} \frac{(q_{re}H)_w}{\rho_{fl} LHV \eta_b} \quad (28)$$

The smaller the payback period, more economical the solution is, which means it needs less time to get back the initial investment by saving fuel.

Optimization

Genetic algorithm multi-objective optimization

A multi-objective problem consists of optimizing (*i. e.* minimizing or maximizing) several objectives simultaneously, with a number of inequality or equality constraints. GA are semi-stochastic methods, based on an analogy with Darwin's laws of natural selection [19]. The first multi-objective GA, called vector evaluated GA (or VEGA), was proposed by Schaffer [20]. An algorithm based on non-dominated sorting was proposed by Srinivas and Deb [21] and called non-dominated sorting genetic-algorithm (NSGA). This was later modified by Deb *et al.* [22] which eliminated higher computational complexity, lack of elitism and the need for specifying the sharing parameter. This algorithm is called NSGA-II which is coupled with the objective functions developed in this study for optimization.

Tournament selection

Each individual competes in exactly two tournaments with randomly selected individuals, a procedure which imitates survival of the fittest in nature.

Crowding distance

The crowding distance metric proposed by Deb [23] was utilized, where the crowding distance of an individual is the perimeter of the rectangle with its nearest neighbors at diagonally opposite corners. So, if individual $X^{(a)}$ and individual $X^{(b)}$ have same rank, each one has a larger crowding distance is better.

Crossover and mutation

Uniform crossover and random uniform mutation are employed to obtain the offspring population. The integer-based uniform crossover operator takes two distinct parent individuals and interchanges each corresponding binary bits with a probability, $0 < p_c < 1$. Following crossover, the mutation operator changes each of the binary bits with a mutation probability, $0 < p_m < 0.5$.

Objective functions, design parameters and constraints

In this study, effectiveness and total cost are considered as two objective functions. Pipe diameter (d_o), pipe length (L_1), numbers of pipes per row (N_T), number of rows (N_L), fin pitch (N_f), and fin length ratio (L_f/d_o) were considered as six design parameters. The design parameters and their range of variation are listed in tab. 1.

The ranges of variation of the design parameters and the studied case are selected such that all the constraints introduced in eqs. 19 for heat transfer coefficient and eqs. 24 for pressure drop friction factor are satisfied. To insure the heat pipe performance all the limitations discussed in section *The heat pipe performance* (eqs. 1, 5-7) were introduced as constraint to the solutions obtained in the optimization procedure such that the minimum of these limitations (as the main design limitation which determines the heat transfer capacity of heat pipe) for the total number of heat pipes, eq. (8a), was compared with the amount of computed heat recovered, eq. (22), and in the case that the

Table 1. The design parameters and their range of variation

Variable	From	To
d_o [mm]	20	40
L_1 [cm]	50	150
N_T	4	10
N_L	4	14
N_f [m^{-1}]	311	421
L_f/d_o	0.35	0.56

amount of computed heat recovered was greater than the heat transfer capacity of heat pipe, the corresponding solution would be omitted.

Case study

The HPHE optimum design parameters were obtained for a residential building with total area of 500 m² located in Tehran city with the mean maximum temperature of 35 °C in the summer and the mean minimum temperature of 0 °C in the winter. The required volume flow rate for the summer was estimated to be 7500 ft³/min (3.5396 m³/s) at the room inside temperature of 25°C and 8000 ft³/min (3.7756 m³/s) for the winter at the room inside temperature 23 °C. The exhaust and inlet fresh air were assumed to be 25% of the required volume flow rates, *i. e.* 1875 ft³/min (0.8849 m³/s) for summer and 2000 ft³/min (0.9439 m³/s) for winter. Operating conditions and the cost function constant values are listed in tab. 2.

Table 2. The operating conditions and cost functions of the HPHE (input data for the model)

	Summer	Winter
Inlet fresh air temperature [°C]	35	0
Exhaust air temperature [°C]	28	20
Working hours	2500	3000
C_A [\$ per m ²]	100	
C_{el} [\$ per MWh] [25]	$20 \cdot 10^{-6}$	
C_{eg} [\$ per m ³] [26]	0.07	
R_v	0.1	
M_s	0.05	
η_{fan}	0.8	
η_B	0.8	
COP	0.8	

thickness of 0.5 mm. The pipe inner to outer diameter was selected 0.85. The longitudinal and transverse tube pitch to outer diameter ratios were set to 2.5.

The thermophysical properties of air such as Prandtl number, viscosity, density and specific heat were considered as temperature dependent.

Discussion and results

Model verification

In order to validate the modeling procedure and results, two groups of verification were performed. For the first group of verification procedure, the heat transfer rate (capacity) for a single heat pipe was estimated and compared with the corresponding values reported in [4, 5, 13] (tab. 3). To be able to compare the computed heat capacity by our modeling code and the reported values in the mentioned references, the input values of those references were used as the input values to our developed simulation program. Those input values are also listed in tab. 3. The comparison of modeling output and the reported results in the mentioned references showed (tab. 3) acceptable difference values (less than 10%).

For the second group of verification procedure, the HPHE effectiveness and pressure drop values were compared with the corresponding values in reference [17]. The specifications of the studied HPHE in reference [17] are listed in tab. 4. These data were used as input values for our simulation code. The effectiveness and the pressure drop values reported in [17] and the corresponding values computed by present modeling procedure are shown in

figs. 4(a, b). The comparison of two figures shows an acceptable mean difference value for both the effectiveness (less than 5%) and the pressure drop (less than 9%).

Table 3. The comparison of heat pipe capacity computed by the modeling procedure presented in this paper and the corresponding values reported in [4, 5,13]

Working fluid	Length of heat pipe [cm]	Internal diameter of the pipe [mm]	Wick structure	Operation temperature range [°C]	Heat exchanger orientation [W]	Reported heat capacity [W]	Computed heat capacity (this paper)	Difference [%]	Reference
Methanol	60	9	1 layer 100 mesh SS	15-55	vertical	84	76	9.5	[4]
R-11	50	10.2	4 layer 100 mesh brass screen	26-40	horizontal	50	46	8	[5]
Water	75	15	2 layer 100 mesh copper	30	horizontal	24.5	24.5	0.1	[13]

Table 4. Specifications of HPHE from [17]

Evaporator and condenser length [m]	0.5
Number of rows in direction of flow	6
Longitudinal pitch [m]	0.03
Transverse pitch	0.05
Fin thickness [m]	0.00035
Fin pitch [m ⁻¹]	393.7

Optimization results

To maximize the effectiveness and to minimize the total cost values, six design parameters including pipe diameter, pipe length, numbers of pipes per row, number of rows, fin pitch and fin length ratio were selected. Design parameters (decision variables) and their range of variations are listed in tab. 1. It should be noticed that the effectiveness of the HPHE was selected as the time average of the effectiveness of the HPHE in the summer (with working hours of H_s) and winter (with working hours of H_w), due to the fact that they had different but close values in cooling and heating modes.

$$\varepsilon = \frac{\varepsilon_s H_s + \varepsilon_w H_w}{H_s + H_w} \quad (29)$$

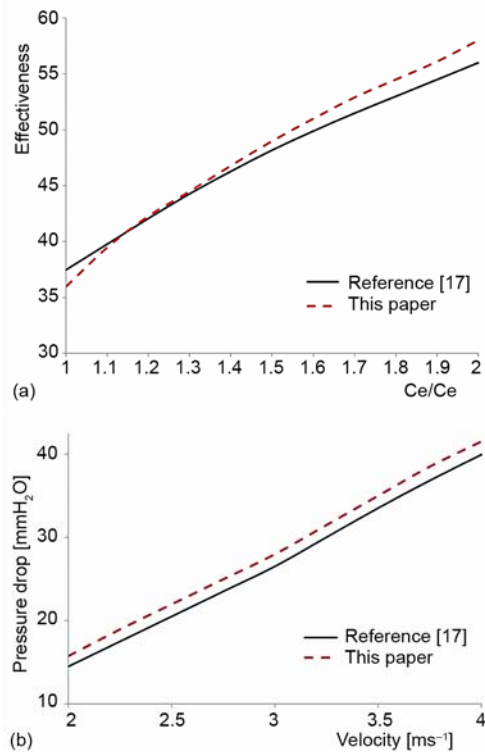


Figure 4. The comparison of heat pipe exchanger (HPHE) (a) effectiveness, and (b) pressure drop computed by the modeling procedure presented in this paper and the corresponding values reported in [17]

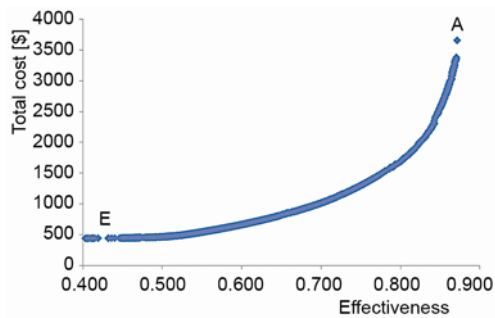


Figure 5. The distribution of Pareto optimum point solutions using NSGA-II

Table 5 The optimum values of effectiveness and the total annual cost for the design points A–E in Pareto optimal fronts for input values given in tab. 1

	A	B	C	D	E
Effectiveness	0.871	0.821	0.700	0.550	0.403
Total cost [\$]	3654	1940	1016	546	444
Payback period [year]	1.66	2.69	2.36	1.89	4.69

Optimum values of two objectives for five typical points from A–E (on Pareto optimal front) as well as payback period for the input values given in tab. 1 are listed in tab. 5. To provide a useful tool for the optimal design of the HPHE, the following equation for the optimal values of effectiveness vs. the total cost was derived for the Pareto curve (fig. 5).

$$C_{\text{tot}}[\$] = \frac{3.59723\varepsilon^2 + 3.42417\varepsilon + 0.80354}{0.41635\varepsilon^4 + 1.11837\varepsilon^3 + 1.13218\varepsilon^2 + 0.50631\varepsilon + 0.08001} \quad (30)$$

Equation (30) is valid in the range of $0.403 < \varepsilon < 0.871$ for effectiveness. The eq. (30) provides the minimum total cost for a desired optimal point. The selection of final solution among the optimum points existing on the Pareto front needs a process of decision-making. In fact, this process is mostly carried out based on engineering experiences and importance of each objective for decision makers. Based on the information provided for designers the practical effectiveness values in the range of $(0.7 < \varepsilon < 0.8)$ the design points (B–C) with reasonable total cost and effectiveness values are recommended. However, because of practical reasons only one optimal solution should be chosen at the end. There are several methods for decision-making process in multi-objective optimization problems. Due to the fact that the dimensions of objectives in our problem are different (the effectiveness is dimensionless, while the total cost is in terms of US dollar), all objectives became non-dimensionalized before decision-making. One of non-dimensionalization methods is Euclidian technique [24] which was employed here. Details of this method can be found in [24]. Therefore, all non-dominated optimal solutions are plotted in non-dimensional form in fig. 6. After Euclidian non-dimensionalization of all objectives, two common types of decision-making process including LINMAP (linear programming technique for multidimensional

System was optimized for depreciation time 15 years and both interest and discount rates equal to 0.1. The genetic algorithm optimization was performed for 100 generations, using a search population size of $M=150$ individuals, crossover probability of $p_c=0.8$ and gene mutation probability of $p_m=0.05$. The results for Pareto-optimal curve are shown in fig. 5, which clearly reveals the conflict between two objectives, the effectiveness and the total cost. Any geometrical change that increases the effectiveness or heat transfer rate, leads to an increase in the total cost and vice versa. This shows the need for multi-objective optimization techniques in optimal design of a HPHE. It is shown in fig. 5, that the maximum effectiveness exists at the design point A (0.871), while the total cost is the biggest at this point (3654 \$). On the other hand the minimum total cost occurs at design point E (444 \$), with the smallest effectiveness value (0.403) at that point.

Optimum values of two objectives for five typical points from A–E (on Pareto optimal

analysis of preference) and TOPSIS (technique for order preference by similarity to an ideal solution) methods were utilized to select the final optimum design point [24]. In LINMAP method, a solution on the Pareto front curve with the minimum special distance from an ideal point (the point at which each single objective has its optimum value regardless of satisfaction of other objectives) was selected as the best optimum design point. In TOPSIS method, in addition to the ideal point, a non-ideal point (the point at which each objective has its worst value) was also defined. In other words, the TOPSIS method not only required that the selected final optimal point should had the shortest distance from the ideal point but also it should had the farthest distance from the non-ideal point.

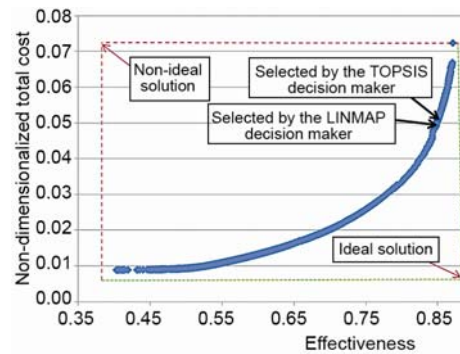


Figure 6. Non-dimensionalized objectives and the selected points due to ideal and non-ideal solutions

Therefore, both solution distance from the ideal point, and non-ideal point were estimated and the solution with maximum value of the closeness coefficient was selected as the best optimal point. The final optimum design points selected by aforementioned methods are marked in fig. 5. Results show that both decision-making methods lead to approximately the same values for the system effectiveness (0.847 and 0.842 for LINMAP and TOPSIS decision-making methods respectively) but 2492 US\$ total cost for LINMAP procedure and 2301 US\$ for TOPSIS method. Hence, the selected point by LINMAP method was considered as the final optimal design point.

In order to see the effect of different inlet fresh air volume flow rates on the optimum solutions which occur in different applications and buildings, optimization with different inlet fresh air volume flow rates has been performed and their Pareto front is shown in fig. 7. The change in the values of design parameters for various inlet fresh air volume flow rates are shown in figs. 8(a)-(d). The outer diameter and the fin height ratio for all cases were at their maximum permissible values as listed in tab. 1. The results show that when the inlet fresh air volume flow rate increases, the pipe length, fig. 8(a) and the number of pipes per row, fig. 8(b) increase while in this situation the number of rows as well as the fin pitch decrease, figs. 8(c) and (d).

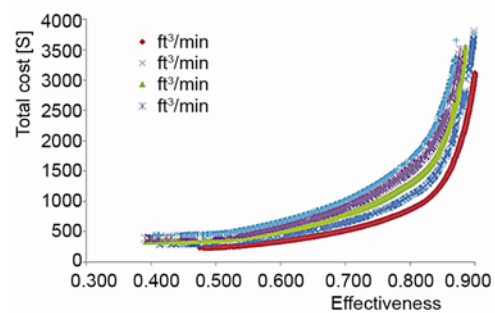


Figure 7. The distribution of Pareto optimum solution points for five different inlet fresh air volume flow rates (ft³/min)

(for color image see journal web-site)

As is shown from fig. 7 for a specific effectiveness value the total cost rises as the inlet fresh air volume flow rate increases. For example the optimum total cost for $\varepsilon = 0.8$ and the inlet fresh air volume flow rate of 4000 ft³/min (1.888 m³/s) is 870 \$ while it is 1693 \$ for 8000 ft³/min (3.776 m³/s). This is due to increase in both pipe length, fig. 8(a) and the total number of pipes, eq. 8(a) as indicated by figs. 8(b, c) which causes to increase the initial investment due to higher surface area (eq. 25) as well as increase in the pressure drop which rises operational cost (eq. 26). It should be noted that the mild decrease of fin pitch with increase

in inlet fresh air volume flow rate, fig. 8(d) had much less effect on the pressure drop and operating cost as well as initial investment and due to the fact that the number of rows decreased but the total number of pipes increased at the same time in this situation. Therefore with higher inlet fresh air volume flow rate in the HPHE system the total cost as well as energy recovered increased (fig. 9) which at the equilibrium point for 4000 ft³/min was 129840 MW/year and for 8000 ft³/min was 259270 MW/year.

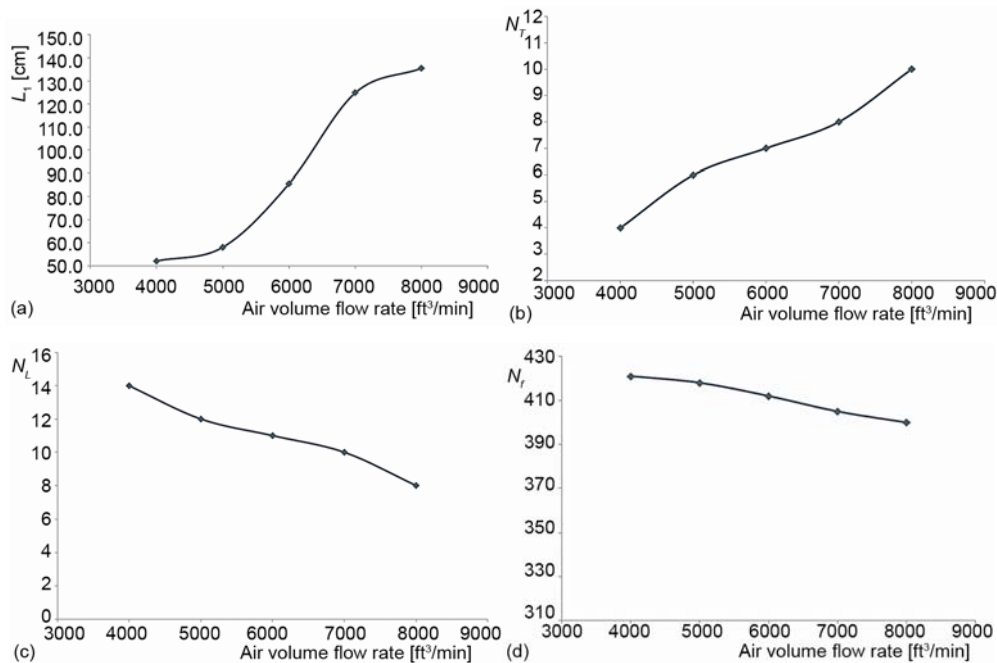


Figure 8. Change of design parameters with the change of inlet fresh air volume flow rates at the equilibrium point;(a) pipe length, (b) number of pipes per row,(c) number of rows, and(d) fin pitch

Figure 10 shows that the payback period decreases with increase in the inlet fresh air volume flow rate. In this situation due to increase in the amount of heat recovered, the fuel saving cost was much more than the increase in the total cost.

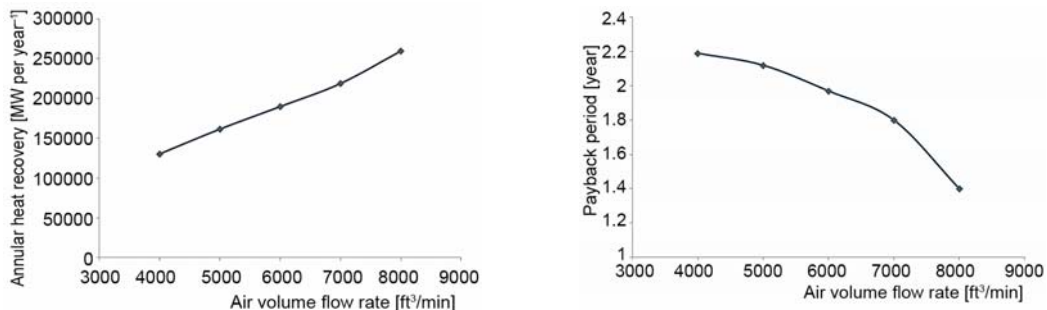


Figure 9. Annular heat recovery of HPHE at the equilibrium point of different inlet fresh air volume flow rates

Figure 10. Payback period at the equilibrium point of different inlet fresh air volume flow rates

Heat pipe performance results

The heat transfer limitations of heat pipe as constraint for the obtained optimum solution points, for five points A-E in fig. 5 as well as total number of heat pipes and the amount of heat recovered are listed in tab. 6. The results show that for the studied system the capillary limit (obtained from eq. 1) had the lowest value among the other limitations for all optimum solution points. This means that none of the boiling, entrainment and sonic limitations caused the heat pipe operation failure.

Table 6. Heat pipe operating limits for five points A-E

	A	B	C	D	E
$q_{cap}[W]$	234.0	238.7	266.7	263.0	313.4
$q_s [W]$	8650.4	8650.4	8650.4	8650.4	8316.0
$q_b[W]$	9197.5	5163.5	4801.8	4687.2	3817.9
$q_{ent}[W]$	6640.4	6640.4	6640.4	6640.4	6383.7
N_{tot}	126	98	80	63	36
$q_{re,s}[W]$	23726.7	229928	20642.6	14224.4	9221.3
$q_{re,w}[W]$	20074.4	18892.1	16012.4	12502.4	9117.6

Conclusions

A heat pipe heat exchanger was optimally designed using multiobjective optimization technique with pipe diameter, pipe length, numbers of pipes per row, number of rows, fin pitch and fin length ratio as design parameters. The effectiveness and total cost were two objective functions (the effectiveness was maximized and total cost was minimized). A set of Pareto optimal front points were shown. The results revealed the level of conflict between the two objectives. Furthermore a correlation between the optimal values of two objective functions was proposed. The final decision was made with the definition of equilibrium point. Five different inlet fresh air volume flow rates were investigated and the heat exchanger was analyzed economically using payback period method. It was shown that by increasing the inlet fresh air volume flow rate the payback period decreased. To insure that the heat pipes function properly, the heat pipe limitations were introduced as constraint for all the solutions.

Nomenclature

- | | | | |
|-----------|--|------------|---|
| A | – surface area, [m ²] | g | – gravitational acceleration, [ms ⁻²] |
| A_{fr} | – minimum free flow area, [m ²] | h_{fg} | – latent heat of vaporization, [Jkg ⁻¹] |
| A_{HX} | – total heat exchanger surface area, [m ²] | h | – coefficient convection heat transfer |
| A_p | – heat pipe surface area, [m ²] | H | – HPHE working hours |
| C | – Mach number dependent coefficient, heat capacity rate, [WC ⁻¹] | i | – inflation rate |
| C^* | – ratio of minimum to maximum heat capacity rates of two streams | k | – thermal conductivity, [Wm ⁻¹ C ⁻¹] |
| C_A | – area dependent cost, [\$m ⁻²] | K_{per} | – wick permeability, [m ²] |
| C_{eg} | – electricity unit cost, [SMW ⁻¹ h ⁻¹] | L | – length |
| C_{el} | – gas price, [\$m ⁻³] | l | – liquid |
| C_{fl} | – fuel saving cost | l^* | – modified length |
| C_{op} | – total operation cost, [\$] | LHV | – lower heating value of methane |
| C_{tot} | – total cost, [\$] | Ms | – ratio of annual maintenance and miscellaneous expenditures to original initial cost |
| COP | – coefficient of performance of refrigeration cycle | \dot{m} | – mass flow rate, [kgs ⁻¹] |
| d | – diameter, [m] | N_f | – fin pitch, [m ⁻¹] |
| ds | – market discount rate | N_L | – number of rows |
| f | – friction factor | N_{mesh} | – screen mesh number, [m ⁻¹] |
| G | – mass velocity, [kgm ⁻² s ⁻¹] | N_p | – payback period time |
| | | NPW | – net present worth |
| | | N_T | – number of pipes per row |

N_{tot}	– total number of heat pipes
N_y	– technical life of HPHE, [year]
NTU	– number of transfer units of HPHE
Nu	– Nusselt number
P	– pipe pitch
ΔP	– pressure difference, [Pa]
PWF	– present worth factor
p_c	– crossover probability
p_m	– mutation probability
Q	– flow rate, [m^3s^{-1}]
q	– heat transferred, [W]
r	– radius, [m]
R	– thermal resistance, [CW^{-1}]
Re	– Reynolds number
Rv	– ratio of resale value to initial cost
r_n	– boiling radius, [m]
s	– parameter defined in eq. (19), [m]
T	– temperature, [C]
t	– thickness, [m]
U	– overall heat transfer coefficient, [WC^{-1}]
v	– vapor
X	– individuals from the genetic algorithm population
x	– parameter to calculate minimum free flow area, [m]
y	– parameter to calculate minimum free flow area, [m]
z	– parameter to calculate minimum free flow area, [m]

Greek symbols

γ	– ratio of specific heats
ε	– effectiveness
η	– efficiency
μ	– viscosity, [Pa.s]
ρ	– density, [kgm^{-3}]
σ	– surface tension, [Nm^{-1}]
φ	– wick porosity
ψ	– heat pipe angle with horizontal

Subscripts

ad	– adiabatic
b	– boiler, boiling
c	– condenser
cap	– capillary
e	– evaporator
eff	– effective
ent	– entrainment
f	– fin
g	– gravitational
i	– inner
in	– inlet
L	– longitudinal
o	– outer
out	– outlet
R	– room
s	– sonic, summer
T	– transverse
tot	– total
w	– winter
wi	– wick

References

- [1] Faghri, A., *Heat Pipe Science and Technology*, Taylor & Francis, Washington D.C., USA, 1995
- [2] Yang, F., *et al.*, Waste Heat Recovery Using Heat Pipe Heat Exchanger for Heating Automobile Using Exhaust Gas, *Applied Thermal Engineering* 23 (2003) 3, pp. 367-372
- [3] Yau, Y. H., Application of a Heat Pipe Heat Exchanger to Dehumidification Enhancement in a HVAC System for Tropical Climates – a Baseline Performance Characteristics Study, *International Journal of Thermal Sciences* 46 (2007), 2, pp. 164-171
- [4] Noie-Baghban, S. H., Majideian, G. R., Waste Heat Recovery Using Heat Pipe Heat Exchanger (HPHE) for Surgery Rooms in Hospitals, *Applied Thermal Engineering* 20 (2000), 14, pp. 1271-1282
- [5] Abd El-Baky, M. A., Mohamed, M. M., Heat Pipe Heat Exchanger for Heat Recovery in Air Conditioning, *Applied Thermal Engineering* 27 (2007), 4, pp. 795-801
- [6] Peretz, R., Bendescu, J., The Influence of the Heat Pipe Heat Exchanger's Geometry on its Heat Transfer Effectiveness, *Heat Recovery Systems* 3 (1983), 1, pp. 23-34
- [7] Tan, J. O., *et al.*, Heat Pipe Heat Exchanger Optimization, *Heat Recovery Systems & CHP* 11 (1991), 1, pp. 313-319
- [8] Soylemez, M. S., On the Thermoeconomical Optimization of Heat Pipe Heat Exchanger HPHE for Waste Heat Recovery, *Energy Conversion and Management* 44 (2003), 15, pp. 2509-2517
- [9] Peretz, R., Horbaniuc, B., Optimal Heat Pipe Heat Exchanger Design, *Heat Recovery Systems* 4 (1984), 1, pp. 9-24
- [10] Sanaye, S., Hajabdollahi, H., Multi-Objective Optimization of Shell and Tube Heat Exchangers, *Applied Thermal Engineering* 30 (2010), 14-15, pp. 1937-1945
- [11] Bejan, A., Kraus, A. D., *Heat Transfer Handbook*, John Wiley and Sons, New York, N. J., USA, 2003

- [12] Peterson, G. P., *An Introduction to Heat Pipes, Modeling, Testing, and Application*, John Wiley and Sons, New York, N. J., USA, 1994
- [13] Kuppan, T., *Heat Exchanger Design Handbook*, Marcel Dekker, New York, USA, 2000
- [14] Incropera, F. P., *et al.*, *Fundamentals of Heat and Mass Transfer*, 6th ed., John Wiley and Sons, New York, N. J., USA, 2006
- [15] Tan, J. O., Liu, C. Y., Predicting the Performance of a Heat-Pipe Heat Exchanger, Using the Effectiveness-NTU Method, *Int. J. Heat and Fluid Flow*, 11 (1990), 4, pp. 376-379
- [16] Kays, W. M., London, A. L., *Compact Heat Exchangers*, 3rd ed., McGraw Hill, New York, USA, 1984
- [17] Azad, E., Geoola, F., A Design Procedure for Gravity-Assisted Heat Pipe Heat Exchanger, *Heat Recovery Systems*, 4 (1984), 2, pp. 101-111
- [18] Duffi, J. A., Beckman, W. A., *Solar Engineering of Thermal Processes*, 3rd ed., John Wiley and Sons, New York, N. J., USA, 2006
- [19] Goldberg, D. E., *Genetic Algorithms in Search, Optimization and Machine Learning*, Addison-Wesley, Reading, Mass., USA, 1989
- [20] Schaffer, J. D., Multiple Objective Optimization with Vector Evaluated Genetic Algorithms, *Proceedings*, 1st International Conference on Genetic Algorithm and Their Applications, Pittsburg, Pens., USA, 1985, pp. 93-100
- [21] Srinivas, N., Deb, K., Multiobjective Optimization Using Nondominated Sorting in Genetic Algorithms, *Journal of Evolutionary Computation*, 2 (1994), 3, pp. 221-248
- [22] Deb, K., *et al.*, A Fast and Elitist Multiobjective Genetic Algorithm: NSGA-II. *IEEE Transactions on Evolutionary Computation*, 6 (2002), 2, pp. 182-197
- [23] Deb, K., *Multi-Objective Optimization Using Evolutionary Algorithms*, John Wiley and Sons, New York, N. J., USA, Chichester, UK, 2001
- [24] Sayyaadi, H., Mehrabipour, R., Efficiency Enhancement of a Gas Turbine Cycle Using an Optimized Tubular, *Energy*, 38 (2012), 1, pp. 362-375
- [25] ***, <http://www.tavanir.org.ir/>
- [26] ***, <http://www.nigc.ir/>